THERMAL SPALLING OF ROCK

L. N. GERMANOVICH
Sarkeys Energy Center, The University of Oklahoma,
100 E. Boyd P119, Norman, OK 73019, USA

ABSTRACT

A two-dimensional micro-mechanical model of massive thermal spalling which results from the localized heating of the surface of a brittle, low porous material (such as many types of ceramic, concrete, glass, and rock) is devised in the paper. While macroscopically the spalling amounts to an advance of the free surface into the material, microscopically thermal spalling can be attributed to successive growth of inherent cracks in the surface layer subjected to high thermoelastic compression. An inclined sub-surface initial flaw ejects branches (wings) which continue to open and propagate as tensile fractures parallel to the direction of compression, that is, parallel to the surface. If the crack is small and suited far from the boundaries, it grows stably; when the crack size becomes comparable to the distance between the crack and free surface, the crack-surface interaction takes over leading to unstable crack propagation. The separated layer eventually buckles resulting in the separation of the spall.

KEY WORDS

Thermal spalling, crack growth, brittle fracture, thermoelastic stresses, rock

1. INTRODUCTION

Brittle breaking by thermal methods has been known to man for many thousands of years. The flame spalling and weakening of rock was used in the Neolithic age and this method applied to driving mine openings was widely employed by the ancient Egyptians (e.g., Rebrik 1984). Therefore, even the ancients had already had a great deal of experimental material and the practical need to study the mechanisms of thermal spalling of rock. However, for natural reasons, the fastest development of this technique became possible only in the twentieth century, and the theory began to take on its present form only in the mid 1950s. Similarly to the past centuries, the main motivation for this development have been in the practical needs and the hope to advance more efficient techniques of rock (materials) treatment and/or fragmentation. Nevertheless, it is probably save to say that the mechanics of this possibly oldest method of fracturing known to the mankind for at least 10,000 years still remains to be fully understood.

If the heating is localized on the body surface, in many cases the failure occurs by the separation of material particles. Such surface adjacent failure is called 'spalling' which is the desirable effect in rock drilling while the main concern of the average ceramist is to prevent the thermal shock damage. A diagram of the process of rock thermal spalling is presented in Fig. 1a. The

separating particles are usually thin plates (flakes), sometimes of irregular shape, significantly smaller than the diameter of the heated spot on the surface (Fig. 1b and 1c). Typically, the spalling is mosaic in nature: particles fly from the surface of flaking in a random manner. Brittle flaking was observed upon heating of rock by supersonic high-temperature gas and plasma jets, microwave and infrared radiation, and by laser and electron beams (e.g., see references in Rauenzahn and Tester, 1989; Germanovich and Gontcharov, 1997). Although below we often refer to the *rock* thermal spalling, the developed model is also applicable to other brittle materials (such as many types of low porous ceramic, concrete, and glass) with chaotically distributed pre-existing microcracks.

In practice, thermal spalling induced by high-temperature gas jets is easier to perform (e.g., Rauenzahn and Tester, 1989) and with an acceptable accuracy, the heat transfer through the body surface can be described as

$$\lambda \frac{\partial T}{\partial n} = \aleph(\Theta - T) \qquad (1)$$

where Θ is the gas temperature, $\aleph$ is the heat transfer coefficient, T is the temperature inside the rock (with respect to the initial temperature of the unheated rock), λ is the thermal conductivity, and n is the external unit vector normal to the surface. Usually, $\Theta \sim 10^3$–10^4 °C, $\aleph \sim 10^2$–10^3 W/(m^2 °C) which corresponds to the initial heat fluxes $Q = \aleph\Theta \sim 10^5$–$10^7$ W/m^2. The velocity of the jet can be up to $\sim 10^3$ m/s. Depending upon the heating parameters, Θ and $\aleph$, the thickness of the particles spalled is $\Delta \sim 0.1$–10 mm, the time required for their separation is $\tau \sim 0.1$–100 sec. The rock surface temperature at the moment of fracture is $T_f \sim 10^2$–10^3 °C, though, naturally, with brittle fracture it remains below the melting point, T_m ($\sim 10^3$ °C for rocks). Note that typically $T_m < \Theta$ (often $T_m << \Theta$) but brittle spalling is still quite stable; indicating that the material does not have enough time to melt so that it flakes before the melting begins and its surface moves inward constantly exposing the cooler areas. For low heat fluxes, $Q = \aleph\Theta \lesssim 10^5$ W/m^2, virtually all hard rock is reliably broken by brittle flaking. However, there are many rocks, called poor thermally spallable, which when heated in regime of $Q \gtrsim 10^6$ W/m^2 spontaneously begin to melt. The linear speed, v, of the spalling front propagation inward the rock is on the order of 1–10 m/hr and depends greatly on the rock type.

In the case of radiation fluxes, the mechanism of their radiation with the matter is usually quite complex and depends upon many factors (e.g., see Prokhorov et al., 1990). The phenomenological (macroscopic) approach to the description of the interaction of radiation with matter is often possible for non-transparent materials and low radiation flux density ($\lesssim 10^4$ W/cm^2). Then the heating process can be described ignoring volumetric nature of heat sources inside the material and assigning instead the heat flux, Q, through the surface:

$$\lambda \frac{\partial T}{\partial n} = Q. \qquad (2)$$

Many works dedicated to the thermal spalling considered the problem of thermoelasticity for a half space utilizing (1) and (2) with non-uniform distributions of temperature or heat flux (e.g., Kill', 1967; Lauriello and Chen, 1973; Germanovich, 1986; Prokhorov et al., 1990). Figure 2 summarizes the results. Typically, the compressive stresses are concentrated in a thin surface layer and drop rapidly from the surface into the depth of the half space. Beneath this layer is a zone of tensile stresses, which change significantly more slowly. If δ is a certain constant having the dimension of length and representing the characteristic "width" of the heated zone, then $\delta >> d$ where d is the typical thickness of the compressed layer. Since spalling occurs in the *compressed* layer, the typical thickness, Δ, of the spalled particles is $\lesssim d$.

Because the thermoelastic compression is concentrated in a narrow surface layer, this fact and the shape of the separated spalls (Fig. 1b) allowed Cherepanov (1966) and Kill' (1967) to assume that final fracture occurs by a mechanism of mechanical buckling *preceded* by the crack growth in a narrow compressed layer. Although after that the mechanisms of crack growth in a thermally compressed layer were somewhat discussed in the literature (Germanovich, 1986; Rauenzahn and Tester, 1989), due to the significant mathematical constraints, quantitative

methods of crack theory have not been utilized in the study of brittle thermal spalling . In this paper, we attempt to devise a simple 2-D micromechanical model of thermal spalling which does not depend, essentially, on the specific heating method used and explicitly accounts for fracture growth in compression.

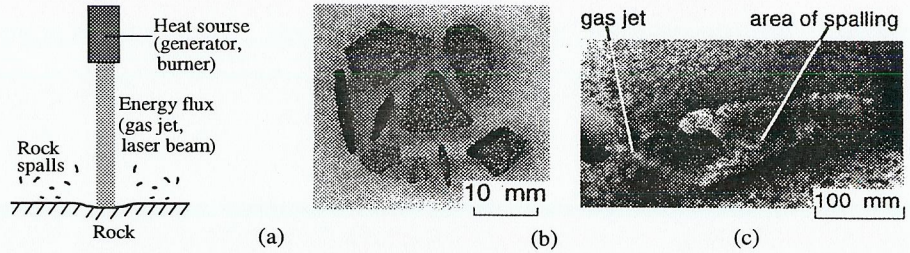

Fig. 1. (a) Diagrams of the processes of thermal fracture, (b) spalled particles of granite, and (c) granite piercing by supersonic high-temperature gas jet.

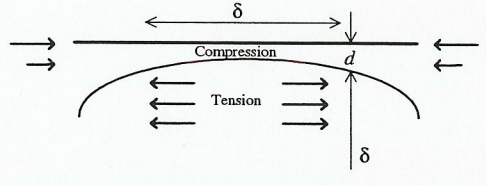

Fig. 2. Schematic representation of thermoelastic stress field in a body heated through a bounded area, δ, on its free surface. Usually, δ >> *d*.

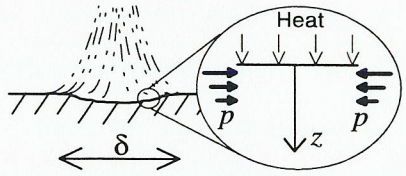

Fig. 3. Global and local scales associated with thermal spalling.

2. GENERAL CONCEPTS

2.1. Global and Local Scales

First, we note that the spalling particles which separate from material as a result of thermal spalling are significantly smaller than the characteristic dimension of the heated area. As mentioned before, particles do not separate simultaneously over the entire surface of the hot spot, but rather follow a mosaic pattern. This indicates the local nature of fracture and usually $\delta >> d \gtrsim \Delta$ (see also Fig. 2). We can introduce a 1-D model to the analysis of small-scale surface spalling in the compressed layer where tensile stresses are negligible (Fig. 3). This model is inapplicable for studying large-scale deep fracture/damage, since the tensile stresses in the area of extension (Fig. 2) appear because of the heating nonuniformity. Therefore, the *global* model of multidimensional heating acts on the scale of the entire heated area while, in contrast, the *local* 1-D model acts on the scale of the flaking particles (Fig. 3).

The stresses near the surface of the heated body are now determined from the solution of the corresponding 1-D thermoelastic problem for the half space (e.g., Germanovich and Gontcharov, 1997):

$$\sigma_{xx} = \sigma_{yy} = -\frac{\alpha E}{1-\nu} T, \quad \sigma_{zz} = 0 \quad (z \gtrsim 0) \qquad (3)$$

where x and y axes are lying on the half-space boundary (Fig. 3); α is the coefficient of linear thermal expansion; E is Young's modulus; and, ν is Poisson's ratio. In (3), temperature, T, is also defined from the local 1-D model. Accordingly, it satisfy the heat conduction equation

$$\frac{\partial T}{\partial t} = a\frac{\partial^2 T}{\partial z^2} \qquad (z>0,\ t>0) \tag{4}$$

with zero initial condition, $T(z, 0) = 0$, and boundary conditions given by (1) or (2) for $-\partial/\partial n = \partial/\partial z$, $z = 0$, and $t > 0$ ($T = 0$ for $z \to \infty$ and $t > 0$). In the case (1) of hot-gas-jet heating,

$$T(z,t) = \Theta\left[\operatorname{erfc}\frac{z}{2\sqrt{at}} - \exp\left(h^2 at + hz\right)\operatorname{erfc}\frac{z+2hat}{2\sqrt{at}}\right], \tag{5}$$

while for the prescribed heat flux (2)

$$T(z,t) = \frac{Q}{\lambda}\left(2\sqrt{\frac{at}{\pi}}\cdot e^{-\frac{z^2}{4at}} - z\cdot\operatorname{erfc}\frac{z}{2\sqrt{at}}\right). \tag{6}$$

Here a is rock thermal diffusivity and $h = \aleph/\lambda$.

2.2. *Crack Propagation in Compression as a Mechanism of Thermal Spalling*

Preston and White (1938) were probably the first who realized the importance of pre-existing flaws extending by the compressive stress field for the mechanism of thermal spalling. However, at that time they could not describe the crack growth in detail. Similarly to the crack located far from the boundary, shear displacement on an inclined near-surface (sub-surface) initial flaw produces tensile stresses at the flaw tips (front). Eventually, the crack branches (wings) formed from single breaks continue to open and propagate as tensile fractures parallel to the direction of compression as shown in Fig. 4. In the test, plates of Tennessee Sandstone (2.5 cm thick) with near-edge slits were subjected to uniaxial compression. Right crack (45°) in Fig. 4 propagated unstably at 21 MPa. Left crack (60°) propagated at 37.3 MPa. Initial cracks were filled by thin plates of aluminum to insure the contact between their sides. This type of crack growth has also been observed by Nemat-Nasser and Horii (1982). The wings shall be oriented parallel to the surface and a growing crack cannot generally turn towards the surface because of the high compression acting between the surface and the crack. This explains how a thin layer subjected to longitudinal compression is separated from the surface (compare Fig. 5). In brittle spalling, the layer finally buckles as the heating proceeds and compression gets greater. Consequently, the result of fracture can be surface flaking, yielding thin plates/spalls (Fig. 1b).

Therefore, while *macroscopically* the fracture amounts to an advance of the free surface into the material, *microscopically* thermal spalling of a brittle material can be attributed to successive growth of pre-existing inherent cracks in the compressive thermoelastic stress field. The separation of the surface layer occurs mach faster (~10^{-3} sec) than its heating (~0.1-10^2 sec) so that the boundary conditions can be considered restored after each separation cycle. Note that the character of crack growth in compression fundamentally depends upon crack location with respect to the body boundaries. Cracks that are suited far from the boundaries, grow stably so that each increment of crack growth requires a stress increase. In contrast, cracks interacting with the nearby surface, propagate unstably. For example, left crack shown in Fig. 4 propagated unstably from the very beginning while the right crack, located further from the plate boundary, had a very short, but noticeable period of stable growth.

The scenario outline above will be quantified further in the paper. However a rigorous analysis is unrealistically complex and we first shall uncouple the problems of heat conduction and crack growth. The simplest way to do this is to consider the crack as located in a confined body with homogeneous temperature. In this case, $K_{II} = O(a_0^{1/2})$. If we wish to consider the heterogeneity of the temperature field, we can approximate it, in the next approximation, by a temperature which depends linearly on coordinates. Placing a crack in such a field, based on the result from Sih (1962), we see that in it $K_{II} = O(a_0^{3/2})$. Therefore, for cracks of small dimensions, we shall

account only for the term considering the temperature as being homogeneous in the vicinity of a crack while addressing its growth. Accordingly, in an attempt to account for the main feature of spalling, crack growth in compression near the free surface, we ignore crack influence on the temperature field. The crack is considered as growing in the stress field, p, defined by (3) where $T(z,t)$ is the temperature (5) or (6) which would be in the intact material.

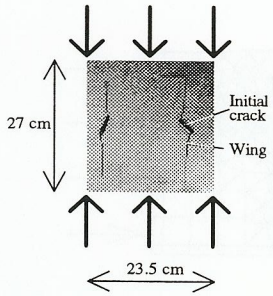

Fig. 4. Sub-surface cracks propagating in compression (see text).

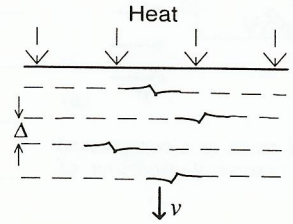

Fig. 5. A mechanism of inward movement of the free surface.

3. A MODEL OF CRACK IN COMPRESSIVE STRESS FIELD

3.1. *Initial Crack Subjected to Compression*

Various problems for a crack in the half-space have been considered in many publications (e.g., Hartranft and Sih, 1973). The problem in question (Fig. 6a) differs from those because of the absence of normal displacement discontinuity on the crack. A simple analytical solution can be obtained using the alternating method (e.g., see Hartranft and Sih, 1973), i.e., by iterations considering the crack in an infinite plane and reflecting the stresses from the line corresponding to the half-plain boundary. This procedure leads to a series with respect to the small parameter, the dimensionless crack length, $\lambda = 2l/\Delta$, where $2l$ and Δ are the crack size and depth, respectively (Fig. 6a). In the case of Coulomb-More friction,

$$K_{II} = \left(\frac{1}{2}p\sin(2\psi) - kp\sin^2(\psi) - C\right)\left[1+\frac{\lambda^2}{16}(2-k\sin\psi)\right]\sqrt{\pi l} \qquad (\lambda \to 0). \tag{7}$$

where k and C are the friction coefficient and cohesion. In (7), the term ~ λ^2, represents only the asymptotic (far field) approximation rather than full crack-boundary interaction. Nevertheless, the "rule of thumb" is (see Dyskin and Mühlhaus, 1995) that the dipole asymptotics are normally applicable even for the values of the relevant parameter (λ in our case) on the order of 1 and even larger than that. Moreover, this additional term (~ λ^2) neither changes the character nor the order of magnitude of K_{II} and, therefore, can be further ignored. For simplicity, we further consider the case of no friction and no cohesion.

We have tested this reasoning against numerical modeling conducted with the finite element code FRANC2D (Wawrzynek and Ingraffea, 1991). We used gap-elements between the crack edges to enforce non-penetration and to allow slip. The fragment of the deformed mesh is shown in Fig. 6b. As a result of this numerical modeling, we obtained that the asymptotic approximation (7) in the case of no interaction ($\lambda = 0$) gives an error of –4.6% and –2.1% for the lower and upper crack tips. This level of inaccuracy is certainly negligible for our purposes. The error could be different for other crack inclinations but within the model of thermal fracture developed here we are looking only at the *average* crack inclined at a certain *average* angle which we approximate at 45°. Hence, even though the crack-boundary interaction has a dramatic effect on crack propagation (section 2.3), *before* it begins the interaction can be ignored.

We can now estimate the stress, p_{cr}, at which the crack will start growing. We assume that at the moment when the crack begins to grow, $K_{II} \approx K_{Ic}$. Since we are considering some typical crack rather than an individual one, we average (7) over the angle ψ and find for $\lambda = 0$:

$$p_{cr} = \sqrt{\frac{\pi}{a_0}}\, K_{Ic}. \qquad (8)$$

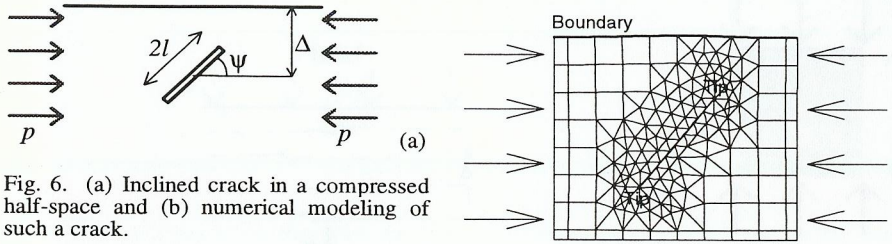

Fig. 6. (a) Inclined crack in a compressed half-space and (b) numerical modeling of such a crack.

3.2. Developed Stage of Crack Growth

The complex geometry of a real wing crack (Fig. 4) does not allow reasonably simple modeling of this crack. Furthermore, as applied to the problem of thermal spalling it is not necessary to account for details of crack growth since we have already made a number of simplifications; most important being the temperature field assumed unaffected by the crack. The quantitative description of the crack growth will be based on a simple model suggested by Fairhurst and Cook (1966) (Fig. 7a). In this model, the growing fracture is modeled by a rectilinear crack opened by a pair of concentrated forces. The value of these effective forces (per unit length of the inclined contact area) is assumed to be equal to the vertical projection of the shear force tending to displace the opposite faces of the initial crack (e.g., Dyskin and Salganik, 1987; Germanovich et al., 1994). This can be expressed as:

$$F = 2a_0 p\beta(\psi), \quad \beta(\psi) = C\sin^2\psi\cos\psi \qquad (9)$$

where p is the applied compressive stress acting along the free surface (Fig. 3); C is a near unity factor accounting for the friction and curvature of the wings.

In the case of a free half-plane boundary, simple approximation formulae for the SIFs for the crack shown in Fig. 7a can be found by matching their asymptotics for great and small crack lengths. For small crack lengths we obviously have

$$K_I \sim K_I^{\infty} = F/\sqrt{\pi l}, \quad K_{II} \to 0 \quad (l/\Delta \to 0). \qquad (10)$$

We shall use the beam approximation method to consider large crack lengths. This method allows to find the rate of elastic energy release, Γ, associated with the crack growth. Looking upon the material above the crack as a beam (plate) with clamped ends and calculating the strain energy, U, of bending this beam (plate), we easily find that

$$\Gamma = \frac{\partial U}{\partial l} \propto k_1^2 + k_2^2 = \frac{3}{8}\left(\frac{l}{h}\right)^3 \quad (l/h \to \infty) \qquad (11)$$

where $k_1 = K_I\sqrt{l/F}$ and $k_2 = K_{II}\sqrt{l/F}$. Furthermore, the results of Zlatin and Khrapkov (1986) allow the ratio of the SIFs to be found with asymptotic accuracy: $k_1/k_2 = 0.78$ $(l/\Delta \to \infty)$. Using (11), we then find the asymptotics

$$k_1\sqrt{\pi} = A\left(\frac{l}{\Delta}\right)^{3/2}, \quad k_2\sqrt{\pi} = -B\left(\frac{l}{\Delta}\right)^{3/2} \quad (l/\Delta \to \infty) \qquad (12)$$

where $A = 0.856$ and $B = 0.668$. Simple interpolation of the asymptotics (10) and (12) for mode I yields the equation

$$k_1\sqrt{\pi} = \frac{K_I}{K_I^{\infty}} = 1 + A\left(\frac{l}{\Delta}\right)^{3/2} \qquad (13)$$

which is asymptotically accurate for both great and small l/Δ [for mode II, we use (12) directly]. A comparison with the results of numerical modeling is shown in Fig. 7b, 7c and demonstrates the agreement which is good enough for most practical situations and certainly for our goals. More accurate asymptotic formulae as well as some justification of beam approximation technique were given by Ustinov et al. (1994).

If there were no free surface, K_{II} would be zero. The non-zero value of K_{II} (Fig. 7c) results from the interaction between the crack and the free surface. According to the conventional criteria for crack propagation direction (e.g., Cherepanov, 1979), this should turn the trajectory of the crack toward the free surface. However, as has been experimentally demonstrated by Nemat-Nasser and Horii (1982) and Dyskin et al. (1994), crack propagation under compression remains parallel to the free boundary (see Fig. 4). Recent experiments of Papamichos et al. (1994) on natural rocks also confirm this statement. This phenomenon can possibly be explained by considering that in reality the high compression acts along the crack suppressing the out-of-crack-plane tension. We should also mention that in any case K_{II} is considerably smaller than K_I up to the moment when the crack starts to grow unstably (Fig. 7c).

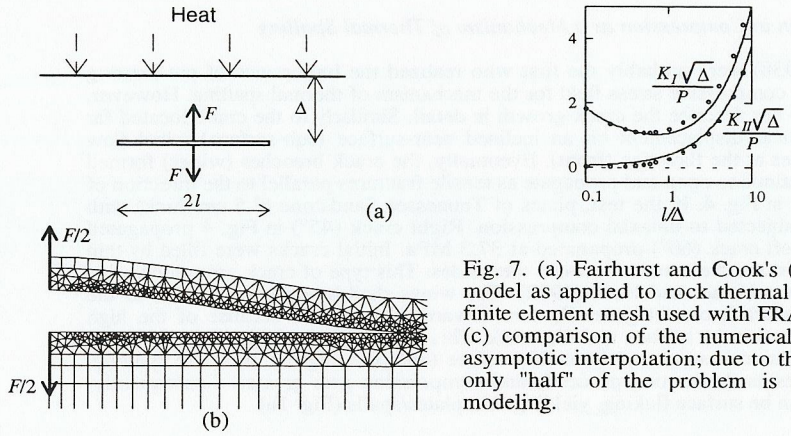

Fig. 7. (a) Fairhurst and Cook's (1966) crack model as applied to rock thermal spalling, (b) finite element mesh used with FRANC2D, and (c) comparison of the numerical results and asymptotic interpolation; due to the symmetry, only "half" of the problem is used in the modeling.

If a crack were located in an infinite plane, the SIF would be given by (10), meaning that the crack could propagate only stably as force F (compressive load) increased. However, as follows from Fig. 7c, dependence of K_I on crack size shows a minimum. Thus, the crack grows unstably where $l > l_{cr} \approx 0.55\Delta$. The corresponding SIF at that point is $K_I = K_I^{\min} = 1.07F/\sqrt{\Delta}$. Substituting this into crack growth condition, $K_I = K_{Ic}$, determines the minimum (critical) force necessary for unstable crack propagation: $F_{cr} \approx K_{Ic}\sqrt{\Delta}$. Using (9) averaged over different angle, ψ, we then obtain the condition of unstable crack growth expressed in terms of applied compressive stress:

$$p_{cr} = \frac{K_{Ic}\sqrt{\Delta}}{2\kappa a_0}, \quad \kappa = \frac{2}{\pi}\int_0^{\pi/2}\beta(\psi)d\psi = \frac{2}{3\pi}. \qquad (14)$$

The magnitude, p, of compressive stress can now be compared to p_{cr} which provides the condition of spalling (see the following section). A rock burst model based on a similar idea was described by Dyskin and Germanovich (1993). The corresponding model of borehole breakouts was discussed by Germanovich et al. (1996).

4. A SIMPLE MICRO-STRUCTURAL MODEL OF THERMAL SPALLING

.1. High Micro-Crack Concentration

Consider material with high concentration of pre-existing cracks, i.e., the case of $\Delta \sim a_0$. At each spalling cycle, the body with a crack is a half-space with a 2-D flaw near the free surface. The most important role of crack-free surface interaction is that crack grows unstably *from the ery beginning*. Therefore, although, for the sake of model simplicity, we ignore this interaction efore crack starts growing, the interaction takes over immediately *after* that moment, τ, making crack propagation unstable.

Let us now introduce the critical temperature, T_g, which must have been reached for a certain micro-crack begin to develop and separate the layer located above it from the surface of the ody (Fig. 5). When the stress (8) is reached, the local development of cracks begins. Using (8), we find that

$$T_g = \sqrt{\frac{\pi}{a_0}}\,\frac{K_{Ic}(1-\nu)}{\alpha E}. \tag{15}$$

Then the layer separation time, τ, is determined by the solution of equation

$$T(\Delta, \tau) = T_g \tag{16}$$

Since in each layer separation cycle the boundary condition (2) and zero initial conditions are assumed to be restored, the expression for temperature is given by (5) or (6). After this the rate of thermal fracture is estimated by $v \approx \Delta/\tau$.

For illustration, we simulated the spalling of magnetite quartzite [$E = 15.12\times10^{10}$ Pa, $\nu = 0.18$, $\alpha = 1.51$ °C^{-1}, $\lambda = 8.2$ W/(m°C), $a = 3.19\times10^{-6}$ m^2/sec, and $K_{Ic} = 1$ MPa·$\sqrt{\text{m}}$; see Germanovich and Gontcharov (1997)] heated by heat flux, Q [condition (2)]. We shall consider a few rock structures which will be modeled by different microcrack dimensions and densities in the rock in scale, δ, of the hot spot. We accept two crack sizes, $2a_0 \approx 1$ mm and $2a_0 \approx 0.1$ mm, comparable to the characteristic grain sizes of the rock. Consider also four anticipated spall thickness: 0.158 mm, 0.5 mm, 1.58 mm, and 5 mm.

The computed rate of advance of the fracture front is shown in Fig. 8a. As we can see, it increases monotonically with increasing heat flux. Figure 8b shows the variation of rock surface temperature at the moment of crack growth. With heat fluxes exceeding 10 MW/m^2 this temperature might be close to the melting point of the rock and the mode of brittle thermal fracture may be unstable. On the other hand, when the heat flux is reduced to 1 MW/m^2 the rate of fracturing is significantly reduced. It can, therefore, be recommended for the reliable brittle thermal fracture of such a rock a mode with heat fluxes of 1-10 MW/m^2. Note that curves 2 and 4 in Fig. 8a and 8b were plotted for the purpose of comparison only since the condition of $\Delta \sim a_0$ is not satisfied for these cases.

4.2. Low Micro-Crack Concentration

Consider the case of lower crack concentrations when a period of stable crack growth precedes its unstable propagation resulting from crack-free surface interaction. We consider the "average" crack, i.e., all cracks are assumed to be the same and modeled by a straight cut opened by a couple of concentrated forces (Fig. 7a). As described in section 2.4, heat conduction only affects the magnitude of remote thermoelsatic stresses which, in turn, define the forces opening the crack. Crack-free surface interaction is reduced to a problem studied in section 4.2 and a crack located at the depth of Δ will grow unstably when the compression at its depth reaches the value of (14). Inserting it in (3), we obtain the temperature,

$$T_{cr} = \frac{p_{cr}(1-\nu)}{\alpha E} = \frac{K_{Ic}(1-\nu)\sqrt{\Delta}}{2\kappa a_0 \alpha E}, \tag{17}$$

of unstable crack growth ($T_{cr} > T_g$). Accordingly, (16) has to be replaced with

$$T(\Delta, \tau) = T_{cr} \tag{18}$$

To be specific, we further consider the case of convective (radiant) heat exchange condition (1) on the free surface so that formula (5) should be used with (18). The temperature distribution at the moment, τ, of the first spall separation is shown in Fig. 9a and 9b (curves 1) for different crack dimensions and heating conditions. As before, magnetite quartzite is employed as an example. In the calculations, we used the order of magnitude values of $a_0 = 0.1$ mm, $L = 1$ mm. As one can see from curves 1, the temperature, T_{cr}, at the bottom of a spall can be quite comparable to the surface temperature, T_f, at the moment, τ, of spalling.

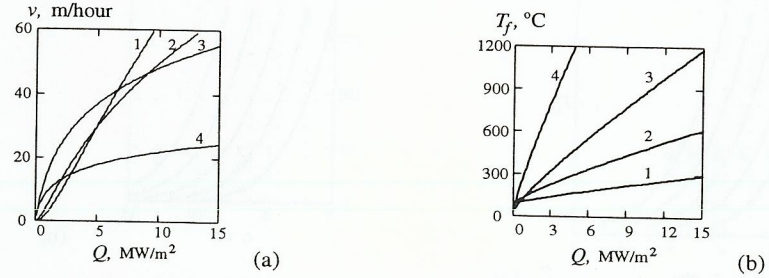

Fig. 8. Dependence of (a) the rate of fracture front advance, v, and (b) the rock surface temperature, T_f, at the moment of crack growth upon the applied heat flux, Q. Four rock structures have been considered: (1) $2a_0 = 0.1$ mm, $\Delta = 0.158$ mm; (2) $2a_0 = 0.1$ mm, $\Delta = 0.5$ mm; (3) $2a_0 = 1$ mm, $\Delta = 1.58$ mm; and, (4) $2a_0 = 1$ mm, $\Delta = 5$ mm.

Hence, building up this model, we cannot *a priori* ignore the residual temperature and stresses in the half-space remaining after the separation of the spall. It is easy though to account for this temperature considering that in our model each spalling represents the surface advance at one step (Fig. 5). Then the temperature at each step will be a superposition of the solutions of the following two boundary value problems for heat conduction equation (4). The first problem has zero initial and non-zero boundary condition (1). The second problem has non-zero initial and zero boundary conditions:

$$T = g(z) \quad (z > 0,\ t = 0), \qquad \frac{\partial T}{\partial z} = hT \quad (z = 0,\ t > 0) \tag{19}$$

where the initial temperature, $g(z)$, at each step is a residual temperature from the previous one. At each step the free surface instantaneously advances one move, Δ, inward the rock, right after the spalling occurs. Having coordinate origin, $z = 0$, attached to the rock surface and counting time from the moment of spalling, we can write that at each step $g(z) = T(z + \Delta, t)$ where $T(z, t)$ is the superposition of the solutions of both problems for the previous step.

The solution for the first problem is given by (5). The solution for conditions (19) is also well known and the total temperature at each step can be expressed as

$$T(z,t) = \Theta f_1(z,t) + \frac{1}{2\sqrt{\pi a \tau}} \int_0^\infty g(\xi)\left\{\exp\left[-\frac{(x-\xi)^2}{4at}\right] + \exp\left[-\frac{(x+\xi)^2}{4at}\right] - 2h\int_0^\infty \exp\left[-\frac{(x+\xi+\eta)^2}{4at} - h\eta\right]\right\} d\eta \tag{20}$$

Finally, we note that at the very first step, $g(x) = 0$ since the rock is supposed to be unheated before the thermal spalling begins.

The integrals in (20) have been calculated numerically. An example of calculations is given in Fig. 9a and 9b where the plots represent temperature distributions in the 2nd, 3rd, 4th, and 5th spalls (curves 2, 3, 4, and 5, respectively) just before their separations, i.e., just prior to flaking. Even though these calculations are not complete, the main observation from this plot is that the temperature gets stabilized after only a few steps of spalling and does not differ too much even from the very first step. This might explain why the modeling based on the initially untreated (unheated) half-space and consideration of just first spalling step is normally representative enough.

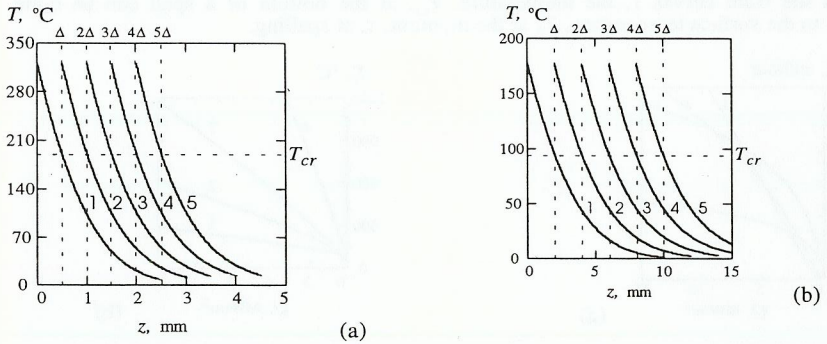

Fig. 9. Temperature distribution in magnetite quartzite before first five spallings (curves 1, 2, 3, 4, and 5, respectively) for two crack sets and heating regimes: (a) $\Theta = 2000$ °C, $\aleph = 1500$ W/(m²·°C), $a_0 = 0.1$ mm, $L = 1$ mm; (b) $\Theta = 1000$ °C, $\aleph = 500$ W/(m²·°C), $a_0 = 0.4$ mm, $L = 4$ mm. Vertical dotted lines indicate the positions of the surface right after each spall separates.

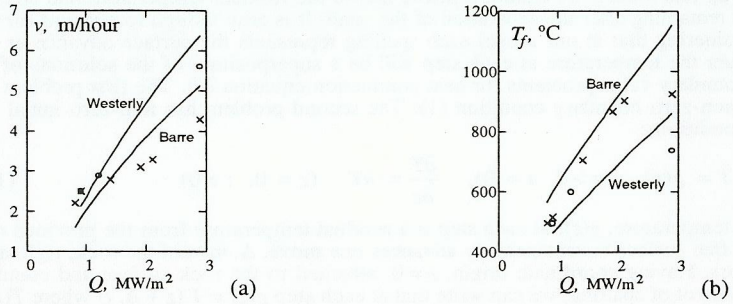

Fig. 10. Comparison of Wilkinson and Tester's (1993) data (crosses for Westerly granite and circles for Barre) with the developed model (curves): (a) velocity of spalling front advance and (b) surface temperature at the moment of spalling.

4.3. Comparison with Test Results

Due to the extremely hostile environment in the spalling area (see section 1.1), the experimental monitoring and accurate measurements of the spalling process are eminently difficult. Although a good amount of observations have been collected, typically, it is only feasible to concentrate on one parameter at a time so that the whole picture is reproduced after mutual efforts of many. In a sense, this whole situation is more typical for Earth sciences rather than for engineering meaning that important constraints are known only in terms of their orders of magnitude. Nevertheless, there is a set of data described by Wilkinson and Tester (1993) which allows its comparison to the model under consideration. Although not being exactly the result of measurements because part of the parameters was estimated based on the mass and energy balances, these estimates took into account various known constraints and the complex interplay between the thermal fracture and the fluid flow in the gas jet.

In particular, the said data set provides the relation between the rate of flame drilling, v, measured surface temperature, T_f, at the moment of spalling, and the average heat flux, Q, coming through the surface into the material used in the testing (Westerly and Barre granites). In Fig. 10a, 10b we plotted the result of the least square fitting (solid lines) to the data (points) of Wilkinson and Tester (1993). Note that the fit was done in the 3-D space of v, T_f, and Q so that Fig. 10a and 10b show (v, Q) and (T_f, Q) cross section of the fitting surface. We used properties of rocks listed in Table 6 of Wilkinson and Tester (1993) while choosing Δ and a_0 as fitting parameters and employing (6) to calculate the temperature. For the case of high initial crack concentration (section 4.1) we could not obtain any reasonable fit which indicated that the crack density was not high. Accordingly, we then tested the scenario of low initial crack density (section 4.2). The values which gave the best fit, shown in Fig. 10, were $\Delta = 0.77$ mm, $a_0 = 0.35$ mm for Westerly granite and $\Delta = 1.1$ mm, $a_0 = 0.56$ mm for Barre granite. Since grains of Barre granite were roughly twice larger than grains of Westerly (Wilkinson and Tester 1993), the obtained values seem to be in a reasonable relation; although their absolute magnitudes should not be overestimated given the uncertainties in the data set.

5. CONCLUSIONS

We formulated a micromechanical scenario of brittle thermal spalling based on crack growth in the highly compressed surface layer (Fig. 5). Needless to say that although this scenario spells out certain features of thermal spalling, it is highly idealized and many details are still missing. Nevertheless, the described model is useful too understand the main features of the thermal spalling. It presents indeed some generic mechanisms of massive thermal spalling which results from the localized heating of the surface of a brittle, low porous material. This kind of heating leads to high thermoelastic compression acting along the surface. The main mechanism of spalling is based on fracture development in compressive stress field. In particular, with this approach the difference between material which is highly and poorly spallable by thermal methods, and the fact that many non-spallable materials can be highly breakable by low heat fluxes (see section 1.1), is explained as follows.

In a material highly spallable by thermal methods, there is a system of smaller cracks that can grow only at high stresses. They are located close to each other and, therefore, close to the surface which is generated as a result of the sequential growth of nearby cracks (Fig. 5) before the material begins to melt. Poorly spallable material only contains a system of larger cracks and although the distance between the cracks is rather great, the material can be heated through at low heat fluxes; the cracks can grow separating the buckling spalls before melting starts on the surface. If, however, the heat flux is high enough, the heating depth becomes much less by the time melting begins at the surface; the large cracks cannot grow on the average, since at their depth the rock is almost unheated and the stresses are small. This shows that thermal spallability depends upon not only the material type but also on the absorbed heat flux; so that the same material can be non-spallable, poorly spallable, or highly spallable if the applied heat flux varies.

ACKNOWLEDGMENT

I am very grateful to K.K. Lee, for his kind permission to use the photograph shown in Fig. 4. Although our testing was partly described in Dyskin et al. (1994), this particular result has not been published yet. I greatly appreciate multiple discussions with D.K. Astakhov, G.P. Cherepanov, A.V. Dyskin, S.A. Gontcharov, I.D. Kill', L.M. Ring, and R.A. Salganik. I would like to also thank S.A. Gontcharov for sending me the photographs shown in Fig. 1b, 1c and D.K. Astakhov for digitizing them. The support of the NSF (grants EEC-9209619, CMS-9622136, and OCE-9626939) and OCAST (contract 5011) is greatly acknowledged.

ERENCES

repanov, G. P. (1966). High-temperature drilling, *J. Appl. Mech. Tech. Ph.*, **7** [6], 82-84.
repanov, G. P. (1979). *Mechanics of brittle fracture*. McGraw Hill, New York.
kin, A. V. and L. N. Germanovich (1993). Model of rock burst caused by cracks growing ear free surface," In: *Rockbursts and Seismicity in Mines* (R.P. Young, ed.), pp. 169-174. alkema Publishers, Rotterdam.
kin, A. V., L. N. Germanovich, A. R., Ingraffea, K. K. Lee and L. M. Ring (1994). Modeling crack propagation in compression. In: *Rock Mechanics* (P.P. Nelson and S.E. aubach eds.), pp. 451-460. Balkema, Rotterdam and Brookfield.
kin, A. V. and H.-B. Mülhaus (1995). Equilibrium bifurcations in dipole asymptotic model f periodic crack arrays. In: *Continuum Models for Materials with Micro-Structure* (H.-B. Mülhaus, ed.), pp. 69-104. John Wiley and Sons, Ltd.
kin, A. V. and R. L. Salganik (1987). Model of dilitancy of brittle materials with cracks nder compression. *Mechanics of Solids*, **22** [6], 165-173.
hurst, C. and N. G. W. Cook (1966). The phenomenon of rock splitting parallel to the direction of maximum compression in the neighborhood of a surface. In: *Proc. First Congr. ntern. Soc. Rock Mech.*, Vol. 1, pp. 687-692. Lisbon.
manovich, L. N. (1986) Temperature stresses in an elastic half space with heat sources. *Mechanics of Solids*, **21** [1], 77-88.
manovich, L. N., R. L. Salganik, A. V. Dyskin, and K. K. Lee (1994). Mechanisms of brittle racture of rock with pre-existing cracks in compression. *PAGEOPH*, **143** [1/2/3], 117-149.
manovich, L. N. and S. A. Goncharov (1997). *Thermomechanics of Rock Fracture.* Gordon nd Breach Publishers, Inc., London, New York, Philadelphia.
manovich, L. N., A. N. Galybin, A. V. Dyskin, A. N. Mokhel and V. Dunayevsky (1996). Borehole stability in laminated rock. In: *Eurock '96* (G. Barla, ed.), pp. 767-776. Balkema, Rotterdam and Brookfield.
tranft, R. J. and G. C. Sih (1973). Alternating method applied to edge and surface crack roblems. In: *Mechanics of Fracture, Vol. 1, Methods of Analysis and Solutions of Crack Problems* (G. C. Sih, ed.), pp. 179-238. Noordhoff International Publishing, Leyden.
, I. D. (1967). Study of rock fracturing under high temperature gas jet impact with applications to drilling in open mines. Ph.D. thesis, Moscow Mining Institute (in Russian).
riello, P. J. and Y. Chen (1973). Thermal fracturing of hard rock. *Transactions of the ASME, Series E, J. of Applied Mechanics,* **40**, 909-914.
nat-Nasser, S. and H Horii (1982). Compression-induced nonplanar crack extension with pplication to splitting, exfoliation, and rockburst. *J. Geoph. Res.*, **87**, [B8], 6805-6821.
amichos, E., J. F. Labuz and I. Vardoulakis (1994). A surface instability deflection apparatus. *Rock Mechanics and Rock Engineering,* **27**, No. 1, pp. 37-56.
ston, F. W. and H. E. White (1938). Observations on spalling. *J. Am. Ceram. Soc.*, **17**, 137.
khorov, A. M., V. I. Konov, I. Ursu and I. N Mihailescu (1990). *Laser Heating of Metals.* Adam Hilger Press, Bristol, Philadelphia and New York.
enzahn, R. M. and J. W. Tester (1989). Rock failure mechanisms of flame-jet thermal spallation drilling—Theory and experimental testing. *Int. J. Rock Mech. Min. Sci. & Geomech. Abstr.,* **26** [5], 381-399.
enzahn, R. M. and J. W. Tester (1991). Numerical simulation and field testing of flame-jet thermal spallation drilling—2. *Int. J. Heat Mass Transfer*, **34** [3], 809-818.
rik, V. M. (1984). *At the cradle of geology and mining*. Nedra Press, Moscow (in Russian).
G. C. (1962). On the singular character of thermal stresses near a crack tip. *Transactions of he ASME, Series E, J. of Applied Mechanics*, **29**, 587-589.
inov, K. B., A. V. Dyskin, and L. N. Germanovich (1994). Asymptotic analysis of extensive rack growth parallel to free boundary. In: *Localized Damage '94*, pp. 623-630. Computational Mechanics Publications, Southampton, Boston.
wrzynek, P. A. and A. R. Ingraffea (1991). *Discrete Modeling of Crack Propagation: Theoretical Aspects and Implementation Issues in Two and Three Dimensions.* Report 91-5. School of Civil and Environmental Engineering, Cornell University, Ithaca.
kinson, M. A. and J. W. Tester (1993). Experimental measurement of surface temperatures during flame-jet induced thermal spallation. *Rock Mechanics and Rock Engng.*, **26**, 29-62.
tin, A. N. and A. A. Khrapkov (1986). A semi-infinite crack parallel to the boundary of the elastic half-plane. *Soviet Physics — Doklady*, **31** [12], 1009-1010.